Int. J. Electrochem. Sci., 11 **(2016)** 8994 – 9006, doi: 10.20964/2016.11.52

International Journal of ELECTROCHEMICAL SCIENCE
www.electrochemsci.org

Co/CoO Nanoparticles/Ag Nanowires/Nitrogen Codoped Electrospun Carbon Nanofibers as Efficient Electrocatalysts for Oxygen Reduction

Supeng Pei[1,2,*], *Zongshang Zhou*[1], *Xiaohong Chen*[2], *Xiongjie Huang*[2], *Tong Liu*[2], *Boyu Cao*[2] *and Fei Wang*[2]

[1] School of Chemical and Environmental Engineering, Shanghai Institute of Technology, Shanghai 201418, China.
[2] School of Chemistry and Chemical Engineering, Shanghai Jiao Tong University, Shanghai 200240, China.
[*]E-mail: peisupeng@126.com

Received: 15 July 2016 / *Accepted:* 14 September 2016 / *Published:* 10 October 2016

Development of efficient electrocatalysts for oxygen reduction reaction (ORR) is of crucial importance to optimize the performance of fuel cells. In this work, Firstly, Ag nanowires (AgNWs) were in-situ embedded in electrospun carbon nanofibers (CNF). Then, Nitrogen and Co/CoO nanoparticles (Co/CoO NPs) were successively codoped into CNF-AgNWs *via* the thermal annealing process, aiming to increase the accessible surface area of CNF-AgNWs and facilitate O_2 diffusion and OH^- transport of the resulting N-CNF-AgNWs-Co/CoO hybrids. It is demonstrated that N-CNF-AgNWs-Co/CoO exhibited excellent electrocatalytic activity for the ORR in alkaline electrolytes, including high onset potential (-0.069 V), high half-wave potential (-0.246 V), and large electron transfer number (~4).

Keywords: Ag nanowires; Co/CoO nanoparticles; nitrogen-doping; carbon nanofibers; oxygen reduction reaction

1. INTRODUCTION

In proton exchange membrane fuel cells (PEMFCs), small-molecule fuels are oxidized at the anode and concurrently oxygen is reduced at the cathode. Oxygen reduction reaction (ORR) is of great importance to metal air batteries and fuel cells. The current bottleneck of fuel cells lies in the sluggish ORR process on the cathode side. Currently, platinum (Pt)-based materials are the most practical electrocatalysts for ORR. The sluggish reduction process, unsatisfactory stability, high cost, and

limited resource of Pt have stimulated extensive exploration of more effective, durable, and inexpensive alternatives. Therefore, replacing Pt by some cheaper metal catalysts is a more essential and promising way[1,2]. Non-Pt catalysts for ORR should have such advantages as higher activity, long-term operation stability, tolerance to poisons, and moreover sustainability. Among these carbon-based non-Pt catalysts, some catalysts based on iron(Fe), cobalt(Co), nickel(Ni) and others have been at a competitive level to Pt[3-14].

On the other hand, carbon nanomaterials also have been extensively investigated, aiming to the replacement of precious Pt systems. Among varying carbon nanomaterials, carbon nanofibers (CNFs) exhibit important characteristics as simplicity of preparation, electronic conductivity, low cost, and high surface area. CNFs were normally used as support materials for different nanomaterials because they can provide uniform dispersion of loaded catalysts, mechanical support, and an electronic continuity, which may affect reaction characteristics of the catalytically active sites[15,16]. Moreover, despite pristine CNFs have no electrocatalytic activity towards ORR, their heteroatom-doped (such as N, P, B, and S) counterparts show tunable electronic arrangement and thus remarkable ORR activity[17-19]. Nitrogen is mostly used as the doping element to modulate the carbon materials. It is known that N-dopants in the carbon skeleton are favorable anchor sites or defects for enhancing particle nucleation and reducing the particle size[20-22]. Moreover, the introduction of N into the carbon matrix can modify its electronic structure, strengthen the interaction between carbon and guest molecules, and endow the carbon with a metal-like “d” band electronic structure to host the reactive species[23,24].

Silver (Ag) has been considered as another alternative to Pt in alkaline fuel cells due to its unique properties and reasonable catalytic activity. Compared with other noble metals, e.g. Pt, gold (Au), and palladium (Pd), Ag is the cheapest. Another important feature of Ag is its ability to reduce O_2 completely into water (4e) within the whole ORR potential window. This is based on the fact that Ag is an excellent catalyst for hydrogen peroxide reduction, oxidation, or disproportionation, so that hydrogen peroxide can hardly escape from its surface[25]. These properties indicate that Ag will be an ideal codopant for carbon based catalysts to improve both the electron conductivity and catalytic efficiency. Herein, Ag nanowires (NWs) were selected due to their less vulnerability to dissolution, Ostwald ripening, aggregation, and subsequent better electrocatalytic stability compared to zero-dimensional nanoparticles[26,27].

In this contribution, CNF-AgNWs composites were prepared by electrospinning of the aqueous mixture of AgNWs and polyacrylonitrile (PAN) and subsequent high-temperature thermal annealing. Melamine was further used as the nitrogen source for the N-doping of CNF-AgNWs, yielding N-CNF-AgNWs hybrids, which were subsequently in-situ doped by Co/CoO nanoparticles (NPs) to afford the resulting N-CNF-AgNWs-Co/CoO electrocatalysts. Herein, Co component was adopted due to its effective catalytic activity towards redox reactions[28,29]. The results indicate that the N-doping of CNF-AgNWs provides a large number of active sites beneficial to the homogeneous in-situ deposition of Co/CoO NPs. Electrochemical analysis suggests that N-CNF-AgNWs-Co/CoO composite exhibits comparable ORR catalytic activity to that of the commercial catalyst of 20% Pt on the carbon black (Pt/C), with a predominant 4e reduction process, more positive onset potential and half-wave potential, due to the synergistic effect between N-CNFs, AgNWs, and Co/CoO NPs.

2. EXPERIMENTAL

2.1 Materials

Melamine, cobalt acetate [$Co(Ac)_2$], and PAN were bought from Sinopharm Chemical Reagent CO.,Ltd. (China). AgNWs were purchased from Nanjing XFNANO Materials Tech Co.,Ltd. 5% Nafion® perfluorinated resin solution was obtained from E. I. DuPont Company (USA). Other chemicals such as ethanol, potassium hydroxide (KOH) and dimethylformamide (DMF) purchased from Shanghai Lingfeng Chemical Reagent CO. Ltd., were all of analytical grade and used as received.

2.2 Synthetic procedures

Preparation of CNFs and CNF-AgNWs

In the DMF solvent, PAN and AgNWs were added to furnish the content of 10% and 0.5%, respectively. Then the mixture was electrospun in the electric fields of the order of 1 kV cm^{-1}. Afterwards, stabilization and carbonization of the above PAN-AgNWs nanofibers were completed in a high-temperature furnace[30], yielding the final CNF-AgNWs hybrids. For comparison, pristine CNFs were also fabricated under the same conditions.

Preparation of N-CNF, N-CNF-AgNWs, N-CNF-Co/CoO, and N-CNF-AgNWs-Co/CoO

CNF-AgNWs and melamine were ground in an agate mortar for 5 min, and the mixture was then placed in the center of a quartz tube under argon flow. With an Argon flow for 20 min, the mixture was heated to 800 ^oC and annealed for 2 h, then was cooled to room temperature to yield the final N-CNF-AgNWs. N-CNF-AgNWs-Co/CoO was prepared from N-CNF-AgNWs and $Co(Ac)_2$ according to the above procedure. N-CNF, N-CNF-AgNWs, and N-CNF-Co/CoO were constructed from CNF by the similar procedure.

Preparation of Pt/C, N-CNF, N-CNF-AgNWs, N-CNF-Co/CoO, and N-CNF-AgNWs-Co/CoO modified electrodes

Prior to use, glassy carbon electrode (GCE, φ = 3 mm) was polished with 0.05 μm gamma alumina powders, then thoroughly rinsed with ethanol and water in an ultrasonic bath to remove any alumina residues, and finally dried at room temperature. 4 μL of 5 mg/mL sonicated Pt/C, N-CNF, N-CNF-AgNWs, N-CNF-Co/CoO, and N-CNF-AgNWs-Co/CoO with 5% Nafion aqueous alcohol solution, ethanol and water suspension was dropped on the pretreated bare GCE or GC disk using a micropipet tip and dried in air.

2.3 Cyclic voltammograms (CV) and electrochemical impedance spectra (EIS) measurements

A conventional cell with a three-electrode configuration was served throughout this work. CV measurement was conducted at 25 ^oC using an Autolab PGSTAT302 (Metrohm) electrochemical test

system using saturated Ag/AgCl as the reference electrode, a Pt wire as the counter electrode and the sample modified glassy carbon electrode as the working electrode. 0.1 M KOH aqueous solution was used as the electrolyte, which was saturated with O_2 by bubbling it prior to the start of each experiment. A flow of O_2 was maintained over the electrolyte during the recording of CVs in order to ensure continuous O_2 saturation. The working electrode was cycled at least 5 times before data recorded at a scan rate of 10 mV s^{-1}. In control experiments, CV measurements were also performed under N_2 atmosphere. In all electrochemical measurements, 0.1 M KOH aqueous solution saturated with nitrogen or oxygen was used as the electrolyte.

EIS was measured according to the above conditions.

2.4 Rotating disk electrode (RDE) and linear sweep voltammetry (LSV) measurements

For the RDE measurement, catalyst inks were prepared by the same method as that of CV analysis described above. 4 μL of 5 mg/mL ink was loaded on a glassy carbon RDE (φ = 3 mm). The working electrode was cathodically scanned at a rate of 5 mV s^{-1} with varying rotating speed from 400 to 2000 rpm. The ORR current was determined by subtracting the N_2 current from the O_2 current. Koutecky-Levich plots (J^{-1} *vs.* $\omega^{-1/2}$) were analyzed at various electrode potentials. The slopes of their best linear fit lines were used to calculate the number of electrons transferred (*n*) on the basis of the Koutecky-Levich equation:

$$\frac{1}{J} = \frac{1}{J_L} + \frac{1}{J_k} = \frac{1}{B\omega^{1/2}} + \frac{1}{J_k}$$

$$B = 0.62nFC_0(D_0)^{2/3}v^{-1/6} \quad J_k = nFkC_0$$

where J is the measured current density, J_K and J_L are the kinetic and diffusion limiting current densities, ω is the angular velocity, n is transferred electron number, F is the Faraday constant (96485 C mol^{-1}), C_o is the bulk concentration of O_2 (1.2×10^{-3} mol cm^{-3}), D_o is the diffusion coefficient of O_2 (1.9×10^{-5}), v is the kinematic viscosity of the electrolyte (0.01 m^2 s^{-1}), and k is the electron-transfer rate constant.

Linear sweep voltammetry(LSV) measurement was carried out in an O_2-saturated 0.1 M KOH electrolyte at a scan rate of 10 mV s-1 using a RDE. In LSV experiment, stable voltammogram cures were recorded after scanning for 5 cycles.

2.5 Apparatus

The morphology of N-CNF, N-CNF-AgNWs, N-CNF-Co/CoO and N-CNF-AgNWs-Co/CoO was characterized by transmission electron microscopy (TEM) and scanning electron microscopy (SEM) using JEM-2010HT and JEOL2100F (both from Electron Optics Laboratory Co., Ltd., Japan), respectively. Powder X-ray diffraction (XRD) analyses were performed on a diffractometer (Bruker, German, APLX-DUO) with Cu Kα radiation. Raman spectra were recorded using a Thermo Fisher H31XYZE-US with an excitation wavelength of 532 nm. X-ray photoelectron spectroscopy (XPS, Kα) analyses were carried out on an AXIS UltraDLD X-ray photoelectron spectrometer system equipped

with Al radiation as a probe, and the analysis spot size was 400 μm in diameter. All the electrochemical measurements were carried out using an Autolab PGSTAT302 (Metrohm) electrochemical workstation.

3. RESULTS AND DISCUSSION

The overall synthetic procedure for N-CNF-AgNWs-Co/CoO hybrids is illustrated in Fig. 1. PAN-AgNWs nanofibers were first obtained *via* electrospinning of the mixture of PAN and AgNWs in DMF. They were then preoxidized and carbonized at 240 and 900 ^{o}C, respectively, affording the CNF-AgNWs hybrids. Subsequently, N-doping of the hybrids and in-situ deposition of Co/CoO on the surface using melamine and $Co(Ac)_2$ as the N and Co sources were sequentially conducted at 800 ^{o}C under argon, yielding the resulting N-CNF-AgNWs-Co/CoO composites.

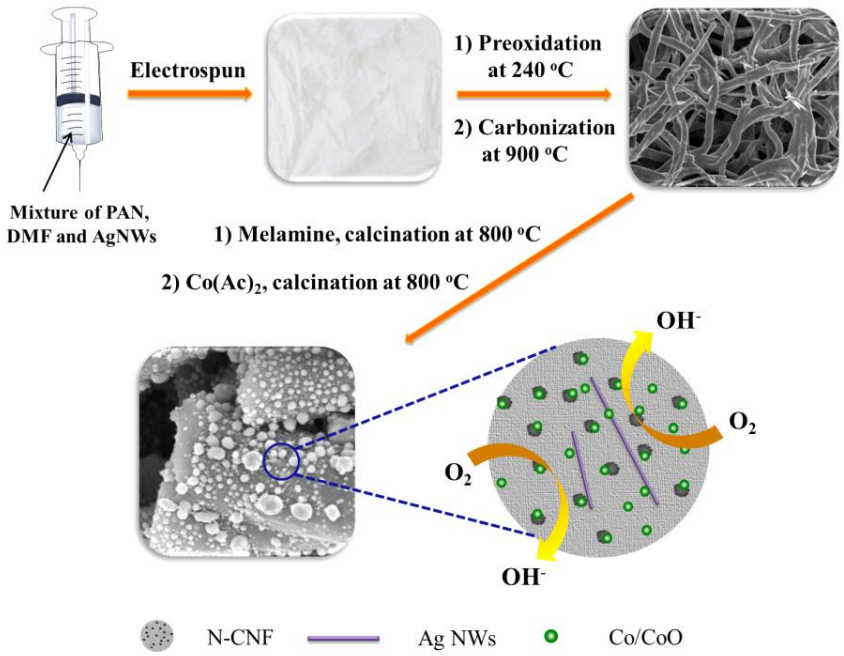

Figure 1. Fabrication procedure for the N-CNF-AgNWs-Co/CoO hybrids

To validate the successful preparation of the hybrids, XRD analysis was conducted. As can be seen from Fig. 2, a peak located around 25.3^{o} is evident for N-CNF, which can be attributed to the graphite (002) crystalline plane with a hexagonal structure. The presence of a few pronounced diffraction peaks at 36.5^{o}, 42.4^{o}, 61.5^{o}, 73.7^{o}, and 77.5 ^{o} (Fig. 2b) can be perfectly assigned to the (111), (200), (220), (311), and (222) planes of CoO, while 44.2^{o}, 51.5^{o}, and 75.9^{o} can be attributed to the (111), (200), and (220) planes of the face centered cubic Co, indicating the formation of Co/CoO on the surface of CNFs. Meanwhile, besides the graphitic diffraction, several peaks located at 38.3^{o}, 44.2^{o}, 64.4^{o}, and 77.4^{o} corresponded to the (111), (200), (220), and (311) crystalline planes of AgNWs with a face-centered cubic (fcc) structure are observed for the N-CNF-AgNWs composite(Fig. 2c)[31]. These peaks are also identified from the diffraction pattern of the resulting N-CNF-AgNWs-Co/CoO

hybrids (Fig. 2d). However, the weak signals of Co/CoO are most likely due to its low crystallinity and the heavy atom effect of silver.

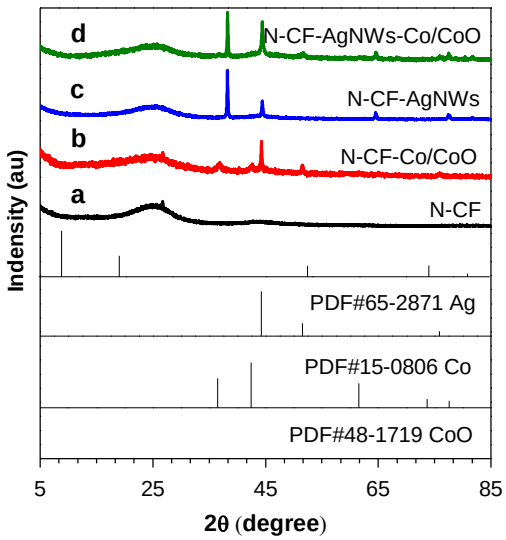

Figure 2. XRD patterns of (a) N-CNF, (b) N-CNF-Co/CoO, (c) N-CNF-AgNWs, and (d) N-CNF-AgNWs-Co/CoO hybrids

Morphologies of N-CNFs and their corresponding hybrids were further revealed by SEM observation. While N-CNFs exhibit smooth surfaces with the diameters ranging from 120 to 240 nm (Fig. 3a), incorporation of AgNWs greatly increases the diameter of the resulting N-CNF-AgNWs (220 to 800 nm) with rough surface. The increase in diameter might be ascribed to the combination of several nanofibers bonded by AgNWs (Fig. 4a, 4b). TEM image discloses the nanoporous structure of the nanofibers with an average pore diameter of 30 nm (Fig. 4c). Such nanopores could provide more active sites for further metal oxide deposition and electrochemical reaction. Energy dispersive spectroscopy (EDS) spectrum (Fig. 4d) indicates the presence of N and Ag elements, thus further confirming the N and Ag doping of the CNFs. When deposited on the N-CNFs, Co/CoO NPs are unevenly dispersed (Fig. 3b), whereas they are relatively homogenously dispersed on the surface of N-CNF-AgNWs with the diameter ranging from 16-140 nm (Fig. 3c). Such greatly improved homogenous distribution of Co/CoO might be resulted from the rough surface of N-CNF-AgNWs, which can provide more nucleation sites for the formation of Co/CoO NPs.

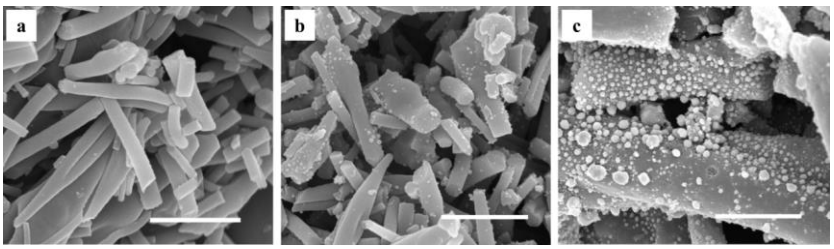

Figure 3. SEM images of (a) N-CNF, (b) N-CNF-Co/CoO and (c) N-CNF-AgNWs-Co/CoO. The scale bar is 1 μm

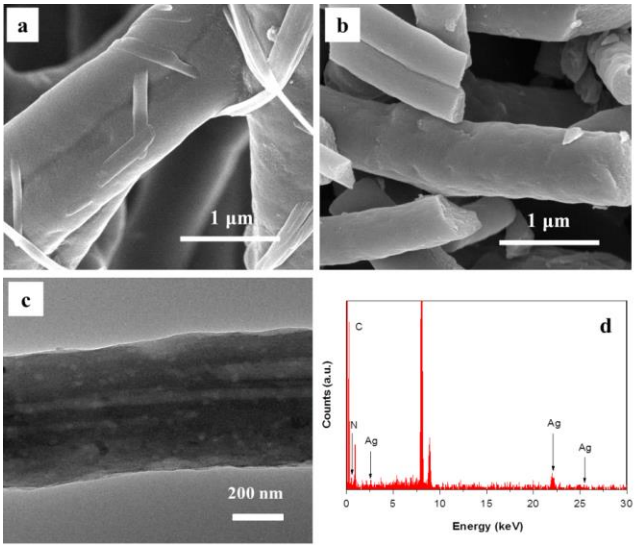

Figure 4. SEM image of (a) CNF-AgNWs and (b) N-CNF-AgNWs. (c) TEM image and (d) EDS spectrum of N-CNF-AgNWs

Raman spectroscopy is a useful tool for the characterization of carbon structure of CNF based materials. As depicted in Fig. 5, two strong bands at around 1347 and 1586 cm^{-1} are observed in both N-CNF-AgNWs and N-CNF-AgNWs-Co/CoO hybrids, which are corresponded to the disordered (D band, defects) and graphitic carbons (G band, E_{2g} mode for sp^2 domains), respectively. It is noted that the area ratio of the D band to the G band (I_D/I_G) for N-CNF-AgNWs-Co/CoO is 1.87, which is much lower than that of N-CNF-AgNWs (2.28), indicating greatly enhanced graphitic structure of the former, which might be mainly attributed to the catalytic graphitization effect of Co element[28]. Such improved graphitic structure would offer enhanced conductivity of N-CNFs, which is favorable for the further electrochemical processes.

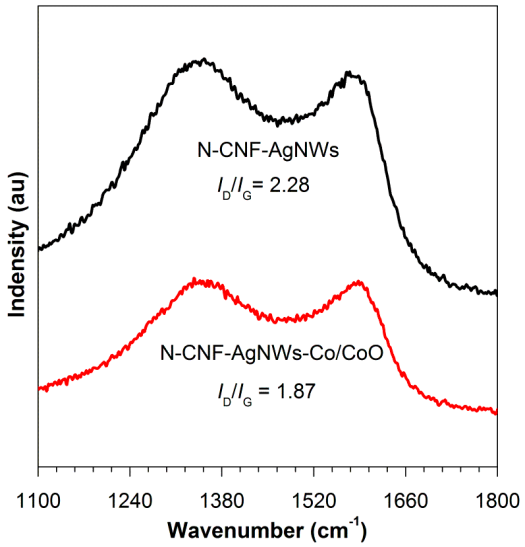

Figure 5. Raman spectra of (a) N-CNF-AgNWs and (b) N-CNF-AgNWs-Co/CoO hybrids

In order to obtain more information of the nitrogen, silver, cobalt, and oxygen functionalities after codoping processes, N-CNF-AgNWs-Co/CoO hybrids were analyzed by XPS. Fig. 6 shows the XPS survey together with the high resolution XPS spectra of N1s, O1s, Ag3d, and Co 2p. Fig. 6a clearly displays intense N1s, O1s, Co2p, and Ag3d peaks, thus verifying the successful codoping of CNFs with surface components of 81% C, 10.69% O, 0.63% Ag, and 4.48% N. It is evident from the N1s deconvoluted peaks (Fig. 6b) that nitrogen is incorporated into the CNFs in three configurations: pyridinic (398.1 eV) (61.5 %), pyrrolic (399.0 eV) (10.8 %), and graphitic (400.9 eV) (27.7 %) nitrogen species. Compared to the pyrrolic and graphitic nitrogen, higher pyridinic nitrogen concentration offers better ORR activity, due to the more geometrically favorable to manage the curvature gradient[32].

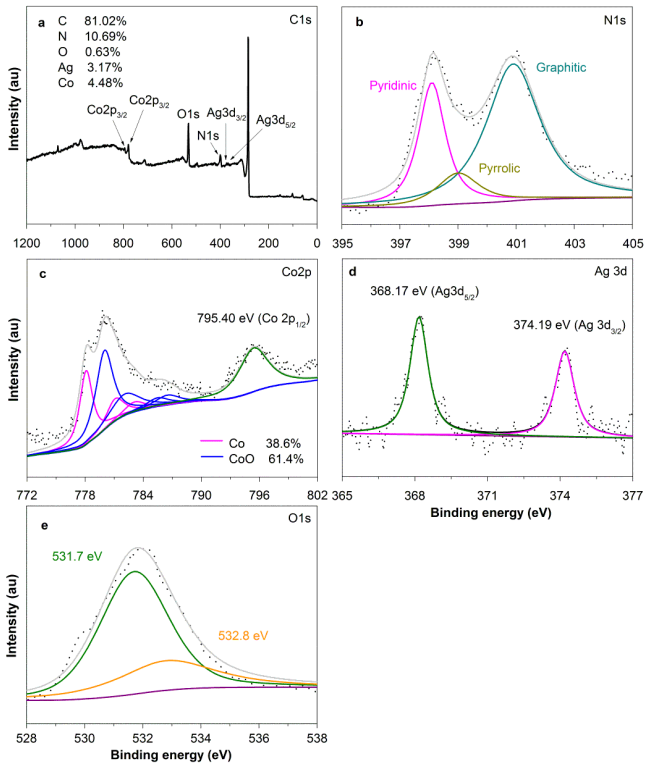

Figure 6. XPS spectra of the (a) survey scan, (b) N1s, (c) Co2p, (d) Ag3d, and (e) O1s regions of the N-CNF-AgNWs-Co/CoO hybrids

Table 1. $Co2p_{3/2}$ spectral fitting parameters: binding energy (eV) and percentage of total area[a]

	P1/eV	%	P2/eV	%	P3/eV	%	P4/eV	%
Co	778.1	61.5	781.1	25.6	783.1	12.8		
CoO	780.0	55.6	782.1	26.6	785.5	8.1	786.5	9.7

[a] P: peak.

Co and CoO spectra are presented in Fig. 6c with spectral fitting parameters given in Table 1, which suggests the fractions of 38.6% and 61.4% for Co and CoO, respectively. Additionally, due to

the higher binding energy $2p_{3/2}$ multiplet or satellite structures of the CoO with the $Co2p_{1/2}$ peak at 795.4 eV, which may effectively cause a slight overestimation of the metal compared to the oxide component[33]. The Ag3d XPS spectrum (Fig. 6d) shows two peaks at 368.2 and 374.2 eV, resulted from $Ag3d_{5/2}$ and $Ag3d_{3/2}$, respectively, which are the same as the standard electron binding energies of metallic silver, indicating that the silver nanowires kept intact during the sample preparation process[34]. The high-resolution O1s XPS spectrum (Fig. 6e) shows both contributions from CoO and CNF. While the peak at 531.7 eV is corresponded to the oxygen species in the CoO phase, that at 532.8 eV are assignable to the residual oxygen containing groups (such as OH and COOH) on the surface of CNFs[35].

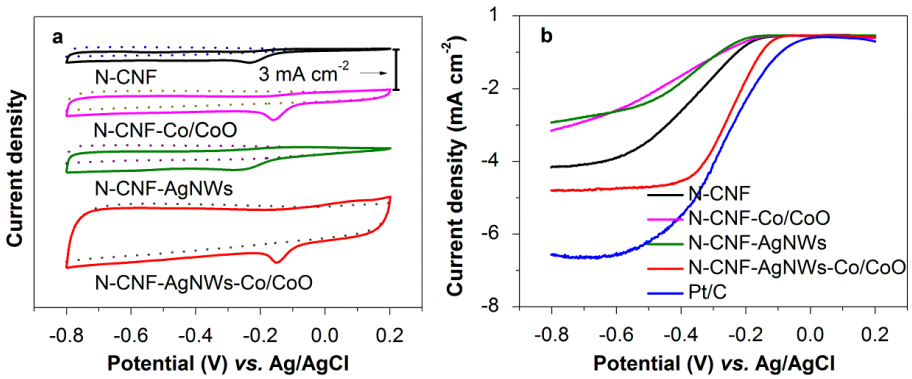

Figure 7. (a) CV curves of the N-CNF, N-CNF-Co/CoO, N-CNF-AgNWs, N-CNF- AgNWs-Co/CoO and Pt/C on glassy carbon electrodes in O_2-saturated (solid line) and N_2-saturated (dot line) 0.1 M KOH at a scan rate of 10 mV s^{-1}. (b) Polarization curves of different samples for ORR in O_2-saturated 0.1 M KOH solution at 298 K. The potential scan rate and the electrode rotation speed were 10 mV s^{-1} and 1600 rpm, respectively. Catalyst loading was ~0.28 mg/cm^2 for all samples

To assess the catalytic activity of these N-CNF-based catalysts for ORR, CV and linear sweep voltammetry（LSV）measurements on a RDE were conducted. The CV curve of N-CNF-AgNWs-Co/CoO shows a peak potential at –0.147 V, which is higher than those of N-CNF (–0.230 V), N-CNF-Co/CoO (–0.161 V), and N-CNF-AgNWs (–0.247 V), suggesting a pronounced and much better electrocatalytic activity of N-CNF-AgNWs-Co/CoO hybrids. Meanwhile, the Fig. 7a indicates a much larger electrochemical surface area and more active sites of N-CNF-AgNWs-Co/CoO. This fact demonstrates the high-density active sites were mainly created by the co-doped AgNWs and Co/CoO NPs on N-CNF, which was similar to some bimetallic catalysts [36]. As depicted in Fig. 7b, N-CNF in 0.1 M KOH exhibits sluggish performance for ORR, as evidenced by its low onset potential of –0.113 V. Compared with pure N-CNF, incorporation of Co/CoO or AgNWs induces slight decline for the ORR process, as indicated by their lower onset potentials of –0.125 and –0.165 V. However, as expected, the onset potential of N-CNF-AgNWs-Co/CoO (–0.069 V) is more positive than that of other three samples, and is more approaching to that of the commercial Pt/C catalyst (–0.014 V), due to the synergetic effect between N-CNF, AgNWs, and Co/CoO NPs. The high ORR electrocatalytic

activity of N-CNF-AgNWs-Co/CoO can also be gleaned from its much higher half-wave potential ($E_{1/2}$, –0.246 V), which is much higher than those of N-CNF (–0.369 V), N-CNF-Co/CoO (–0.436 V), N-CNF-AgNWs (–0.393 V), and even Pt/C (–0.27 V).

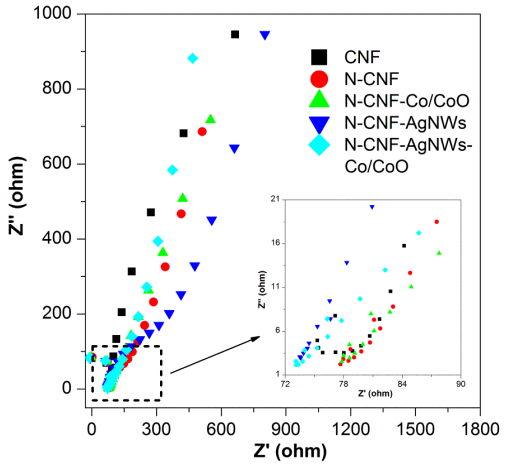

Figure 8. Electrochemical impedance spectra of CNF, N-CNF, N-CNF-Co/CoO, N-CNF-AgNWs, andN-CNF-AgNWs-Co/CoO at 0.3 V vs Ag/AgCl,Cl^{-1}

Table 2. Summary of electrochemical impedance performance of different samples

	CNF	N-CNF	N-CNF-Co/CoO	N-CNF-AgNWs	N-CNF-AgNWs-Co/CoO
Resistance (ohm)	80.68	77.51	76.59	72.51	71.75

Fig. 8 shows the electrochemical impedance spectra of the electrode prepared with CNF, N-CNF, N-CNF-Co/CoO, N-CNF-AgNWs, and N-CNF-AgNWs-Co/CoO, respectively. The low resistance of N-CNF-AgNWs-Co/CoO (Table 2) indicates its better charge conductivity, which may arise from heteroatom-doping induced charge transfer in carbon and the high electrical conductivity of AgNWs[37]. Such good charge conductivity of N-CNF-AgNWs-Co/CoO also testifies the intimate interplay between N-CNF, AgNWs, and Co/CoO is crucial to achieve high electrocatalytic activity.

The reaction kinetics of varying electrodes were further estimated by LSV tests, which were carried out in an O_2-saturated 0.1 M KOH electrolyte at a scan rate of 10 mV s^{-1} using a RDE. The linearity of the Koutecky-Levich plots and near parallelism of the fitting lines are suggestive of the electron transfer numbers (n) for ORR at different potentials (Fig. 9b-d). Derived from the plot slopes, the n values for N-CNF, N-CNF-Co/CoO, and N-CNF-AgNWs are 3.74, 3.91, and 2.79 at –0.8 V, respectively, showing a decreasing tendency due to the reduction of specific surface area of different materials. And the n value for N-CNF-AgNWs-Co/CoO was calculated to be 3.94 at –0.8 V (Fig. 9a and inset), close to that of Pt/C (n = 4), suggesting N-CNF-AgNWs-Co/CoO hybrids favor a 4e oxygen reduction process, which could be attributed to the increase of oxygen diffusion coefficient in the microenvironment of the catalyst layer or the exposure of more active sites on the their surface as the literature has expounded[38]. The E_0, $E_{1/2}$, and n values of varying catalysts are summarized in Table

3. Clearly, the N-CNF-AgNWs-Co/CoO composites exhibit the best comprehensive ORR performance, rendering the hybrids highly potential for future electrocatalytic applications.

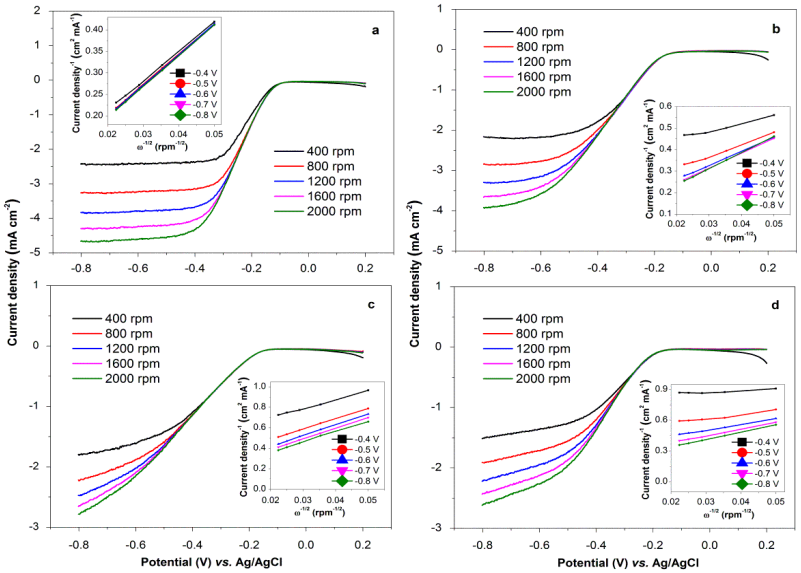

Figure 9. LSV curves of (a) N-CNF-AgNWs-Co/CoO, (b) N-CNF, (c) N-CNF-Co/CoO, and (d) N-CNF-AgNWs in O_2-saturated 0.1 M KOH solution with a sweep rate of 10 mV s^{-1} at different rotation rates. The insets are the corresponding Koutecky-Levich plots derived from the RDE curves at –0.4 ~ –0.8 V

Table 3. Summary of ORR performance of different samples[a]

	E_O (V)	$E_{1/2}$ (V)	n
N-CNF	-0.113	-0.369	3.74
N-CNF-Co/CoO	-0.125	-0.436	3.91
N-CNF-AgNWs	-0.165	-0.393	2.79
N-CNF-AgNWs-Co/CoO	-0.069	-0.246	3.94
Pt/C	-0.014	-0.270	4

[a] E_O: onset potential; $E_{1/2}$: half-wave potential; n: electron transfer number.

4. CONCLUSIONS

In summary, N-CNF-AgNWs-Co/CoO hybrids were successfully fabricated *via* the electrospinning and thermal annealing process. Due to the combined effect of N-CNF, AgNWs, and Co/CoO NPs, the resulting N-CNF-AgNWs-Co/CoO hybrids show excellent electrocatalytic activity for the ORR in alkaline electrolytes, including much higher onset potential, half-wave potential, and electron transfer number (~4), making them promising non-Pt cathode catalyst for fuel cells. Thus, this contribution provides an efficient method for the fabrication of metal oxide nanocomposites and metal nanowires on CNFs, and the application of these catalysts in the fuel cells, which may also potentially be used in supercapacitors or other electrochemical devices.

ACKNOWLEDGEMENTS
We acknowledge National Natural Science Foundation of China (Project No. 21203118).

References

1. R. Bashyam, P Zelenay, *Nature*, 443 (2006) 63.
2. J. W. Liu, J. X. Q, Y. Q. M, J. R. Chen, *J. Mater. Sci.*, 43 (2008) 6285.
3. M. Lefèvre, E. Proietti, F. Jaouen, J. P Dodelet, *Science*, 324 (2009) 71.
4. H. Yano, M. Kataoka, H. Yamashita, H. Uchida, M. Watanabe, *Langmui*r, 23 (2007) 6438.
5. Z. Yang, X. M. Zhou, Z. P. Jin, Z. Liu, H. G. Nie, S. M. Huang, *Adv. Mater.*,26 (2014) 3156.
6. B. Wang, *J. Power Sources*,152 (2005) 1.
7. J. Wu, Y Xue, X Yan, W. S. Yan, Q. M. Cheng, Y. Xie, *Nano. Res.*, 5 (2005) 521.
8. S. J. Guo, S. H. Sun, *J. Am. Chem. Soc.*,134 (2012) 2492.
9. Y. Y Liang, Y. G. Li, H. L. Wang, J. G. Zhou, J. Wang, T. Regier, H. J Dai, *Nat. Mater.*, 10 (2011) 780.
10. R. F. Nie, J. J. Shi, W. C. Du, W. S. Ning, Z. Y. Hou, F. S. Xiao, *J. Mater. Chem. A*, 1 (2013) 9037.
11. W. H. Niu, L. G. Li, X. J. Liu, N. Wang, J. Liu, W. J. Zhou, Z. H. Tang, S. W. Chen, *J. Am. Chem. Soc.*, 137 (2015) 5555.
12. C. W. B. Bezerra, L. Zhang, K. C. Lee, H. S. Liu, A. L. B. Marques, E. P. Marques, H. J. Wang, J. J. Zhang, *Electrochim. Acta.*, 53 (2008) 4937.
13. T. S. Olson, S. Pylypenko, P. Atanassov, K. Asazawa, K. Yamada, H. Tanaka, *J. Phys. Chem. C*, 114 (2010) 5049.
14. Q. F. Yi, Y. H. Zhang, X. P. Liu, B. L. X, Y. H. Yang, *J. Mater. Sci.*, 49 (2014) 729.
15. A. M. Al-Enizi, A. A. Elzatahry, A. R. I. Soliman, S. S. Al-Theyab, Int J *Electrochem. Sci.*, 7 (2012) 12646.
16. H. S. Abdo, K. A. Khalil, S. S. Al-Deyab, H. Altaleb, E. M. Sherif, *Fibers. Polym.*, 14 (2013) 1985.
17. X. Q. Wang, J. S. Lee, Q. Zhu, J. Liu, Y. Wang, S. Dai, *Chem. Mater.*, 22 (2010) 2178.
18. Z. J. Wang, R. R. Jia, J. F. Zheng, J. H. Zhao, L. Li, J. L. Song, Z. P. Zhu, *ACS Nano.*, 5 (2011) 1677.
19. S. Kundu, T. C. Nagaiah, W. Xia, Y. M. Wang, S. V. Dommele, J. H. Bitter, M. Santa, G. Grundmeier, M. Bron, W. Schuhmann, M. Muhler, *J. Phys. Chem. C*, 113 (2009) 14302.
20. K. P. Gong, F. Du, Z. H. Xia, M. Durstock, L. M. Dai, *Science*, 323 (2009) 760
21. D. Usachov, O. Vilkov, A. Gruneis, D. Haberer, A. Fedorov, V. K. Adamchuk, A. B. Preobrajenski, P. Dudin, A. Barinov, M. Oehzelt, C.A.Laubschat, D.V. Vyalikh, *Nano. Lett.*, 11 (2011) 5401.
22. H. Wang, T. Maiyalagan, X. Wang, *ACS Catal.*, 2 (2012) 781.
23. Y. J. Gao, G. Hu, J. Zhong, Z. J. Shi, Y. S. Zhu, D. S. Su, J. G. Wang, X. H. Bao, D. Ma, *Angew. Chem. Int. Ed.*, 52 (2013) 2109.
24. S. K. Movahed, M. Dabiri, A Bazgir, *Appl. Catal. A*, 488 (2014) 26.
25. Y. Z. Lu, Y.C. Wang, W. Chen, *J. Power Sources*, 196 (2011) 3033.
26. R. Zhou, S. Z. Qiao, *Chem. Mater.*, 26 (2014) 5868.
27. D. B. Yu, J. F. Yao, L. Qiu, Y. Z. Wu, L.X. Li, Y. Feng, Q. Liu, D. Li, H. T. Wang, *RSC Adv.*, 3 (2013) 11552.
28. U. Wiedwald, K. Fauth, M. Heßler, H. G. Boyen, F. Weigl, M. Hilgendorff, M. Giersig, G. Schütz, P. Ziemann, M. Farle, *Chem. Phys. Chem.*, 6 (2005) 2522.
29. S. J. Guo, S. Zhang, L. H. Wu, S. H. Sun, *Angew. Chem.*, 124 (2012) 11940.
30. C. N. Wang, H. R. Gao, H. Li, Y. R. Zhang, B. W. Huang, J. H. Zhao, Y. Zhu, W. Z. Yuan, Y. M. Zhang, *Nanoscale*, 6 (2014) 1377.

31. M. A. Kostowskyj, R. J. Gilliam, D. W. Kirk, S. J. Thorpe, *Int. J. Hydrogen Energy*, 33 (2008) 5773.
32. Y. Ito, H. J. Qiu, T. Fujita, Y. Tanabe, K. Tanigaki, M. Chen, *Adv. Mater.*, 26 (2014) 4145.
33. M. C. Biesinger, B. P. Payne, A. P. Grosvenor, L. W. Lau, A. R. Gerson, R. S. C. Smart, *Appl. Surf. Sci.*, 257 (2011) 2717.
34. D. D.Yu, J. Bai, H.O Liang, J. Z Wang, C. P. Li, *Appl. Surf. Sci*., 349 (2015) 241.
35. J. H. Zhou, Z. J. Sui, J. Zhu, P. Li, D. Chen, Y. C. Dai, W. K. Yuan, *Carbon*, 45 (2007) 785.
36. J. S. Huang, H. Q. Hou, T. Y. You, *Electrochem. Commun*., 11 (2009) 1281.
37. H. W. Liang, W. J. Zhang, Y. N. Ma, X. Cao, Q. F. Guan, W. P. Xu, S. H. Yu. *ACS Nano*., 5 (2011) 8148.
38. Jing. Liu, X.J. Sun, P. Song，Y. W. Zhang. W. Xing, W. L. Xu, *Adv. Mater*., 25 (2013) 6879.